Nanoscale Horizons

Probing the Spin Spiral in Fe Chains on Ir(001) using Magnetic Exchange Force Microscopy

Journal:	*Nanoscale Horizons*
Manuscript ID	NH-COM-03-2025-000162.R1
Article Type:	Communication
Date Submitted by the Author:	02-May-2025

Complete List of Authors:	Adachi, Yuuki; The University of Tokyo Graduate School of Frontier Sciences Yasui, Yuuki; The University of Tokyo Graduate School of Frontier Sciences Iiyama, Atsushi; The University of Tokyo Graduate School of Frontier Sciences Kurahashi, Wataru; The University of Tokyo Graduate School of Frontier Sciences Nagase, Rihito; The University of Tokyo Graduate School of Engineering School of Engineering Sugimoto, Yoshiaki; The University of Tokyo Graduate School of Frontier Sciences

SCHOLARONE™
Manuscripts

Spintronics, or spin-transport electronics, utilizes the spin degrees of freedom in condensed matter systems to improve information-processing technology, which has traditionally relied on electric charge. In this work, we introduce a new concept for reading spin states by demonstrating magnetic exchange force microscopy as a method to read out spin information in a finite one-dimensional Fe chain through ferromagnetic coupling between the Fe tip and the Fe chain. This approach differs from existing methods by providing a charge-independent means of accessing spin states at atomic resolution, making it fundamentally distinct from conventional spintronic readout techniques that often rely on optical methods at the macroscopic scale. Moreover, we find that the detected spin information remains robust against chemical interactions with the Fe tip, highlighting the viability of this technique as a nonintrusive spin readout tool. This finding offers additional insights for developing purely spin-based information technologies, thereby advancing the frontiers of nanoscience and nanotechnology.

Journal Name

ARTICLE TYPE

Cite this: DOI: 00.0000/xxxxxxxxxx

Probing the Spin Spiral in Fe Chains on Ir(001) using Magnetic Exchange Force Microscopy†

Yuuki Adachi,[a] Yuuki Yasui,[a], Atsushi Iiyama[a], Wataru Kurahashi[a], Rihito Nagase[a] and Yoshiaki Sugimoto*[a]

Received Date
Accepted Date

DOI: 00.0000/xxxxxxxxxx

The collective motion of spin textures in atomic-scale one-dimensional systems enables information transmission with low electrical current at the nanometer scale. While reading such spin textures with current-free methods is essential for miniaturized spin-based schemes, directly probing them without relying on electrical techniques remains a significant challenge. In this study, we probed the spin texture in one-dimensional Fe chains on Ir(001) using magnetic exchange force microscopy. At large tip-sample distances, we found that ferromagnetic coupling with the tip apex magnetic atoms enables the readout of the spin texture in the Fe chain. At small tip-sample distances, we found that the spin texture in the Fe chain remained robust against chemical interactions within our measurement regime. Our ability to locally detect spins in a one-dimensional structure may pave the way for examining spin information as it propagates between the input and output of miniaturized spin logic devices.

1 Introduction

Magnetism in atomic-scale one-dimensional systems is a rapidly growing research field, offering exciting opportunities ranging from technological applications to the exploration of novel quantum phases [1–8]. In spintronics, atomic-scale one-dimensional systems contribute to the realization of miniaturized spin devices, where the collective motion of spin textures often serves as a connection between inputs and outputs in logic devices, enabling information transport without significant dissipative currents associated with electronic charge [1,3,9]. While spin textures have been probed using current-free methods on the macroscopic scale, direct experimental probing of spin textures in atomic-scale one-dimensional structures without relying on an electric current remains largely unexplored. [10–12].

Magnetic exchange force microscopy (MExFM) is one of the fascinating tools for studying magnetic interactions at the atomic scale using a magnetic tip [13–22]. This method provides information on magnetic interactions that are commonly interpreted as direct exchange interactions ($J\mathbf{S_1}\cdot\mathbf{S_2}$), where J is the coupling constant between two spins $\mathbf{S_1}$ and $\mathbf{S_2}$ [23–26]. This coupling constant J determines the preferred alignment between the magnetic moments, whether they are parallel (ferromagnetic) or antiparallel (antiferromagnetic). [26–28]. However, MExFM has only been applied to a limited number of surfaces, including antiferromagnetic structures (Fe/W and NiO) [13–18], and spiral structures (magnetic skyrmions and Mn/W) [19–22].

To demonstrate the ability to read the spin information in a one-dimensional structure with less electric current, in this study, we perform simultaneous MExFM and SP-STM imaging on the spin spiral in the one-dimensional biatomic Fe chain on Ir(001) [3,29–31]. We employ a Fe tip fabricated by picking up several Fe atoms from the surface. This approach results in a weaker stray field compared to using Fe-coated tips [13,32]. By directly comparing the magnetic contrast in MExFM to that of SP-STM, at large tip-sample distances, we determine the ferromagnetic interaction between the Fe tip and the Fe chain spins.

At small tip-sample distances, the frequency shift contrast reveals chemical interactions, while the tunneling current signal distinctly displays magnetic contrasts, indicating that Fe spins remain robust against chemical interactions. Such robustness implies that the spin spiral can transfer information from one end of the chain to the other, even when the Fe tip is in chemical contact with the Fe chain. To the best of our knowledge, MExFM has not been performed on one-dimensional nanostructures thus far.

2 Results

Figure 1a presents a large-area STM topography image of Fe chains on Ir(001), obtained using a W tip. A large terrace (width

[a] The University of Tokyo Department of Advanced Materials Science, The University of Tokyo, Kashiwa, Chiba 277-8561, Japan

† Supplementary Information available: [details of any supplementary information available should be included here]. See DOI: 00.0000/00000000.

‡ Additional footnotes to the title and authors can be included *e.g.* 'Present address:' or 'These authors contributed equally to this work' as above using the symbols: ‡, §, and ¶. Please place the appropriate symbol next to the author's name and include a `\footnotetext` entry in the the correct place in the list.

$\sim$100 nm) features a regular arrangement of parallel trenches running along the [1$\bar{1}$0] direction. The distance between two adjacent trenches is approximately 1.35 nm (see inset in Figure 1a), consistent with previous studies[3,31]. Due to these trenches, the reconstructed Ir(001) surface is an ideal template for growing self-organized one-dimensional nanostructures. As shown in previous results, the small coverage (less than 20 % - 25 % of atomic layer) of Fe results in growth solely in the trenches, forming biatomic chains[33]. Figure 1b illustrates the area highlighted by the pink dashed line in Figure 1a. To investigate the atomic structure of the Fe chain, we conducted dynamic force microscopy (DFM) imaging. The W tip was carefully approached above the Fe chain, and a DFM image was acquired in constant-height mode in a repulsive regime. Figure 1c displays a frequency-shift (Δf) image. The bright contrast of the Fe chain relative to the Ir substrate indicates that the Fe chain protrudes from the surface. In Figure 1c, for the first time, we experimentally achieved atomic resolution of the Fe chain on Ir(001) using DFM. Figures 1d and 1e show line profiles derived from the Δf image. As seen in Figures 1d and 1e, the distances between Fe atoms along the Fe chain axis is 270 pm, and across the chain is 290 pm.

Next, we present the SP-STM images obtained by picking up several Fe atoms from the surface to the tip apex (see supporting information)[13,32]. A similar method has been employed in previous SP-STM experiments[4,13,32,34]. Figure 2a shows the STM image of the target Fe chain acquired using the W tip. This same Fe chain was subsequently scanned using the Fe tip (Figure 2b). The magnetization of the Fe tip aligns with an external magnetic field in an upward direction due to the superparamagnetic nature of the Fe cluster[32]. Figure 2e presents an enlarged image of the topographic height shown in Figure 2b. In Figure 2e, a periodic structure with a length of three atomic distances of Fe atoms ($\sim$ 0.83 nm $\simeq$ 0.27 nm $\times$ 3) is observed in the Fe chain. This periodicity corresponds well with the magnetic structure of the spin spiral reported in previous SP-STM studies conducted with a W tip coated with a thin Fe film[3,31]. The reproducibility of SP-STM using different tips and various Fe chains is illustrated in Figure S1 and Figure S2. Hence, we conclude that the spin spiral in the Fe chain was successfully observed using the stable magnetic tip fabricated by picking up Fe atoms. It is important to note that Figure 2e was obtained in constant-current mode under an upward external magnetic field of 3.0 T. Thus, the maxima and minima along the chain axis in the topographic height indicate positions where the magnetization components point up and down relative to the external magnetic field, respectively (see Figures S2 and S3 for the chain length and bias voltage dependence of magnetic contrast). When the external magnetic field was ramped to 0.0 T (3.0 T $\rightarrow$ 0.0 T), the periodic structure was barely visible, as shown in Figure 2c (see Figure S4 for the dependence of magnetic contrast on external magnetic fields). In previous experiments, these observations were attributed to fast thermal switching in the orientation of the spin spiral, which cannot be captured by the slow scan of STM[3,31]. After ramping the external magnetic field back to 3.0 T (0.0 T $\rightarrow$ 3.0 T), the magnetic contrast reappeared, as shown in Figure 2d. In Figure 2d, the lateral positions of the maxima and minima along the chain axis in the topographic height are qualitatively similar to those in Figure 2b.

Before discussing the distance dependence of the tunneling current and frequency-shift images of SP-STM and MExFM shown in Figure 4, we present, in Figure 3, the distance dependence of the tunneling current and frequency-shift signals, which were simultaneously obtained on top of the Fe chain by oscillating the tip. Note that we define the distance at the point conductance $G_0 = 7.748 \times 10^{-5}$ S as $z_d = 0$ nm throughout Figures 3 and 4 ($z_d = 0$ nm is the lowest turnaround point of the tip oscillation cycle; see the supporting information for the definition of z_d). Figure 3a presents the tunneling current at the lowest turnaround point of the tip oscillation cycle versus distance curves ($I_{\mathrm{deconvolved}}(z_d)$) obtained on top of the Fe chain. $I_{\mathrm{deconvolved}}(z_d)$ is derived from the deconvolution of the time-averaged tip oscillation of $I(z_d)$[35,36]. In Figure 3a, an exponential dependence is observed in $I_{\mathrm{deconvolved}}(z_d)$. Figure 3b displays $\Delta f_{\mathrm{Fe\,chain}}(z_d)$ simultaneously recorded with $I(z_d)$ in Figure 3a, and $\Delta f_{\mathrm{Ir}}(z_d)$ obtained on the Ir surface. In previous research on antiferromagnetic or spin spiral surfaces, subtracting the long-range components from Δf (z) might be challenging because the first layer of the surface is thoroughly covered with Fe or Mn atoms[19,21,21]. However, in this study, the dark contrast of the Fe chain is identifiable in the DFM image (see inset in Figure 3a), which allows us to obtain $\Delta f_{\mathrm{SR}}(z_d)$ by subtracting $\Delta f_{\mathrm{Ir}}(z_d)$ from $\Delta f_{\mathrm{Fe\,chain}}(z_d)$ (see Figure S5). Figure 3c shows the short-range force $F_{\mathrm{SR}}(z_d)$ deduced from $\Delta f_{\mathrm{SR}}(z_d)$ ($\Delta f_{\mathrm{SR}}(z_d) = \Delta f_{\mathrm{Fe\,chain}}(z_d) - \Delta f_{\mathrm{Ir}}(z_d)$) using the Sader formula[37] (see Figure S5). The potential energy $U(z_d)$, shown in Figure 3d, is further deduced by integrating $F_{\mathrm{SR}}(z_d)$ in the z_d direction. In Figures 3c and 3d, we observe that $F_{\mathrm{SR}}(z_d)$ and $U(z_d)$ monotonically decrease as the tip approaches the surface, clarifying the attractive interaction.

Now, we present the simultaneous observation of MExFM and SP-STM images of the Fe chain[19,21]; see full data sets in Figure S6. Note that Figure 4 was obtained using the same tip as shown in Figure 3. First, we confirm the Fe chain using constant-current mode SP-STM without oscillating the magnetic tip, as shown in Figure 4a. The image was obtained under an upward external magnetic field of 3.0 T, where maxima and minima along the chain axis indicate positions with magnetization components pointing up and down relative to the surface, respectively (see Figure 4h). The same Fe chain was then imaged by oscillating the magnetic tip in constant-height mode at large tip-sample distance ($z_d = 0.284$ nm), medium tip-sample distance ($z_d = 0.149$ nm), and small tip-sample distance ($z_d = 0.069$ nm), with the tunneling current (I) and the Δf signals recorded simultaneously, as shown in Figures 4b and 4c, 4d and 4e, and 4f and 4g, respectively. The black arrows in Figure 3c indicate the tip height at which Figures 4b-4g were obtained. To qualitatively assess the dominant effects in the signals, we normalized the I and Δf signals as $I_{\mathrm{normalized}}$ and $\Delta f_{\mathrm{normalized}}$ in Figures 4(i-k) (the definitions of $I_{\mathrm{normalized}}$ and $\Delta f_{\mathrm{normalized}}$ are provided in the supporting information).

Considering the large tip-sample distance in Figure 4i, the maxima and minima of the $I_{\mathrm{normalized}}$ signal (blue curve in Figure 4i) along the chain axis indicate the magnetization components pointing up and down, respectively, in agreement with their apparent height in the constant-current SP-STM image in Figure 4a

(see also Figure 4h). On the other hand, we observe small corrugation in $\Delta f_{\mathrm{normalized}}(x)$ along the Fe chain (black curve in Figure 4i). The lateral positions of the minima and maxima of the corrugation in $\Delta f_{\mathrm{normalized}}(x)$ agree well with the lateral positions of the maxima and minima in $I_{\mathrm{normalized}}(x)$. Moreover, the large tip-sample distance ($z_{\mathrm{d}} = 0.284\,\mathrm{nm}$) corresponds to the attractive force regime (see Figure 3c). Thus, the $\Delta f_{\mathrm{normalized}}$ contrast suggests ferromagnetic coupling, which increases with the alignment of spins at the tip apex and those at the Fe chain (Figure 4(l)). Furthermore, we demonstrate the observation of ferromagnetic coupling using different tips on different Fe chain, as shown in Figure S7.

Now, we focus on the medium and small tip-sample distances to discuss the effect of the chemical interaction between the Fe tip and the Fe chain. The tip height is decreased until an individual Fe atom might be seen in the Δf image (Figure 4d - Figure 4g). Focusing on the $I_{\mathrm{normalized}}$ signals (blue curves in Figure 4j and Figure 4k), the magnetic contrast is observed at the medium tip-sample distances (blue curve in Figure 4j), while both chemical and magnetic contrasts are evident at the small tip-sample distance (blue curve in Figure 4k). In contrast, in the $\Delta f_{\mathrm{normalized}}$ signal, the chemical contrast dominates rather than the magnetic contrast as the tip-sample distance decreases (black curve in Figure 4i - Figure 4k). Individual surface atoms were imaged in the Δf signal by detecting the short-range forces associated with the onset of the chemical bond between the foremost tip atom and the surface atoms[38,39]. We identified 19 atoms from the leftmost dotted line to the rightmost dotted line, corresponding to 6 spin periods in Figure 4k. Hence, we conclude that the magnetic structure and atomic lattices are incommensurate. Such an incommensurate Fe chain is in good agreement with previous results[29].

Upon comparing Figure 3c, Figure 3d and the constant-height images in Figure 4b - Figure 4g, we find ferromagnetic coupling at F_{SR} ($z_{\mathrm{d}} = 0.284\,\mathrm{nm}$) $\simeq -0.09\,\mathrm{nN}$, and the atomic contrast at $F_{\mathrm{SR}}(z_{\mathrm{d}} = 0.069\,\mathrm{nm}) \simeq -0.75\,\mathrm{nN}$. The short-range force value of $F_{\mathrm{SR}} \simeq -0.75\,\mathrm{nN}$ at $z_{\mathrm{d}} = 0.069\,\mathrm{nm}$ is comparable to those measured in previous results on metallic surfaces using a metal tip[40].

For the potential energy, ferromagnetic coupling is observed at U ($z_{\mathrm{d}} = 0.284\,\mathrm{nm}$) $\simeq -0.05\,\mathrm{eV}$, and the atomic contrast at U ($z_{\mathrm{d}} = 0.069\,\mathrm{nm}$) $\simeq -0.44\,\mathrm{eV}$. The simultaneous observation of the chemical contrast in $\Delta f_{\mathrm{normalized}}$ and the magnetic contrast in $I_{\mathrm{normalized}}$ in Figure 4k (at $z_{\mathrm{d}} = 0.069\,\mathrm{nm}$) suggests that the Fe spins are robust against chemical interactions within our measurement regime. Therefore, the potential energy of $U \simeq -0.44\,\mathrm{eV}$ at $z_{\mathrm{d}} \sim 0.069\,\mathrm{nm}$ indicates that the spin spiral is robust under such strong chemical interaction. Such robustness demonstrates that the spin spiral can transport information from one end of the chain to the other, even when the Fe tip is in chemical interaction with the Fe chain. This property is important for applications as it prevents unintended changes in the information being transferred.

3 Discussion

Here, we discuss several possible mechanisms for interpreting ferromagnetic couplings between the Fe tip and the Fe chain spins. The first interpretation is that the direct exchange interaction occurs between Fe atoms in the Fe tip $\mathbf{S_{Fe\,tip}}$ and in the Fe chain $\mathbf{S_{Fe\,chain}}$, where $\mathbf{S_{Fe\,tip}}$ is the spin in the Fe tip and $\mathbf{S_{Fe\,chain}}$ is the spin in the Fe chain ($J\mathbf{S_{Fe\,tip}} \cdot \mathbf{S_{Fe\,chain}}$). The Bethe-Slater curve indicates that ferromagnetic interaction is favored for a large atomic spacing, while antiferromagnetic interaction is stabilized at smaller atomic spacing[24,26,27]. In Figures 3 and 4, we found ferromagnetic coupling at $z_{\mathrm{d}} = 0.284\,\mathrm{nm}$ (Figure 4(l)). Accordingly, the ratio of atomic separation to the diameter of the $3d$ orbital in our experiment ($0.284\,\mathrm{nm} + d_{\mathrm{Fe}})/d_{\mathrm{Fe}} \sim 2.8$ (assuming the Fe diameter as $d_{\mathrm{Fe}} = 0.158\,\mathrm{nm}$) is sufficiently larger than the distance of the antiferromagnetic coupling in the Bethe-Slater curve[26].

It can be interpreted that there is an indirect interaction between two neighboring Fe atoms with unpaired $3d$ electrons via $4s$ conduction electrons. Such an interaction has been theoretically studied by Tao, K. et al. for an STM with a Cr tip positioned above a magnetic atom protruding from the surface[41]. At large tip-sample distances, ferromagnetic indirect coupling increases; however, at small tip-sample distances, d-d covalent admixture leads to antiferromagnetic interaction[41–43]. This interpretation is consistent with the ferromagnetic coupling observed by MExFM at large tip-sample distances in our experiment. We found ferromagnetic coupling at $z_{\mathrm{d}} \simeq 0.284\,\mathrm{nm}$. Accordingly, the atomic separation of $0.284\,\mathrm{nm} + d_{\mathrm{Fe}} = 0.442\,\mathrm{nm}$ in our experiment is comparable to the tip-sample distance of ferromagnetic coupling observed with the Cr tip. Performing DFT calculations that consider the Fe tip, Fe chain, and Ir surface may facilitate a more detailed quantitative comparison with experimental results. However, we tentatively interpret our experimental results as including both direct exchange interactions and indirect interactions. Moreover, the quantitative evaluation of the magnetic interactions with the distance, as performed in previous works[15,19,21], allows us to determine the magnetic exchange force between Fe tip and Fe chain. Magnetic exchange forces can be extracted from the frequency shift curves as a function of the tip-surface distance, recorded at the maxima and minima of the magnetic contrast in MExFM images of the Fe chain. Such a study could expand our understanding of the interaction between the Fe chain and the Fe tip. However, the observed frequency shift contrasts at large tip-sample distances in Figure 4(c) and S7(b) still directly indicate that the interaction between the Fe tip and the Fe chain is due to ferromagnetic coupling. Thus, we conclude that ferromagnetic coupling at large tip-sample distances plays a key role in reading the spin information of Fe chains on Ir(001).

Conclusions

In summary, we probed the spin information using MExFM on one-dimensional Fe chains on Ir(001). Our results demonstrate ferromagnetic interaction at a large tip-sample distance and chemical interaction at a small tip-sample distance. Such ferromagnetic interaction enables us to read out the spin information in the Fe chain. Looking ahead, we believe that MExFM can be utilized to read spin information in a one-dimensional structure with controlled input, potentially extending its application to new magnetic devices.

4 Graphics

Author contributions

Conceptualization: Y.S., Y.Y., Y.A. AFM, and STM observation: Y.A., A.I., W.K., R.N. Writing original draft: Y.A. Writing review and editing: Y.A., Y.Y., Y.S.

Conflicts of interest

There are no conflicts to declare.

Data availability

The data supporting this article have been included as part of the ESI.

Acknowledgements

We thank T. Ozaki and M. Fukuda for the discussions. This work was supported by JST FOREST Program Grant Number JPMJFR203J and JSPS KAKENHI Grants No. JP24H01175, No. JP23K13656, No. JP22H04496, No. JP20H05849, No. JP21K18867, and No. JP22H01950. Y.S. acknowledges the support of the Asahi Glass Foundation and the Murata Science Foundation. Y.A. acknowledges the support of the Iketani Science and Technology Foundation.

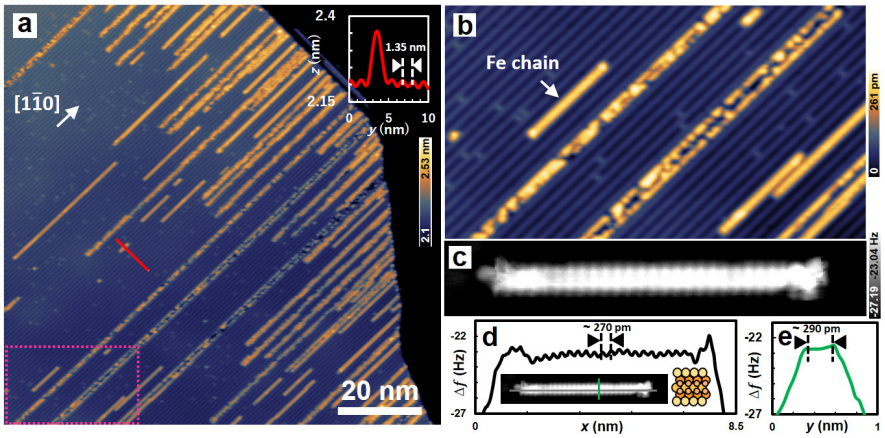

Fig. 1 (a) STM topography image of Fe chains on Ir(001), which forms on the (5 × 1) - reconstructed Ir (001) surface. Note that incomplete/discontinuous Fe chains are the surface alloy. Imaging condition: Constant-current mode. $I = 0.1\,\mathrm{nA}$, $V = 600\,\mathrm{mV}$, $T = 4.5\,\mathrm{K}$ and $B = 3.0\,\mathrm{T}$. Inset: line profile measured above the Ir (001) across the Fe chain as indicated by red color. (b) Enlarged STM topography image of Fe chain within pink dashed box in (a). (c) High-resolution AFM image of the bi-atomic Fe chain obtained by the W tip. Imaging condition: Constant-height mode. $V = 1.0\,\mathrm{mV}$, $T = 4.5\,\mathrm{K}$ and $B = 2.0\,\mathrm{T}$. (d,e) Line profiles obtained from the Δf image in (c). The position of the profiles are shown in the inset by (d) gray and (e) green with a ball model of a bi-atomic Fe chain.

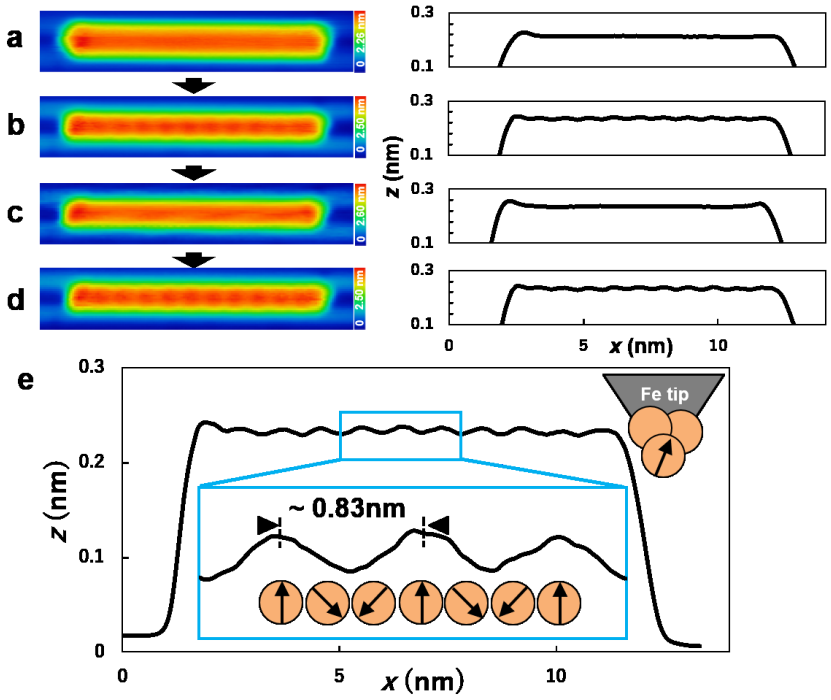

Fig. 2 (a-d) Consecutive STM topography image and the corresponding line profile of Fe chain on Ir(001). Imaging condition: Constant-current mode. $I = 3.0\,\mathrm{nA}$, $V = 600\,\mathrm{mV}$, $T = 4.5\,\mathrm{K}$, (a) $B = 3.0\,\mathrm{T}$; (b) $B = 3.0\,\mathrm{T}$; (c) $B = 0.0\,\mathrm{T}$; (d) $B = 3.0\,\mathrm{T}$. Note that (a) and (b) were both obtained at $3.0\,\mathrm{T}$, but with different tip conditions: (a) was acquired using an W tip, while (b) was acquired using an Fe tip, resulting in different tip states. (b)–(d), on the other hand, were obtained using the same Fe tip condition, with the magnetic field varied as $3.0\,\mathrm{T}$, $0.0\,\mathrm{T}$, and $3.0\,\mathrm{T}$, respectively. (e) Enlarged image of $z(x)$ in (b) with a schematic of spin spiral in Fe chain and Fe tip. The schematics of the spin spiral are validated under similar experimental conditions, as reported in Ref. [3] and Ref. [31].

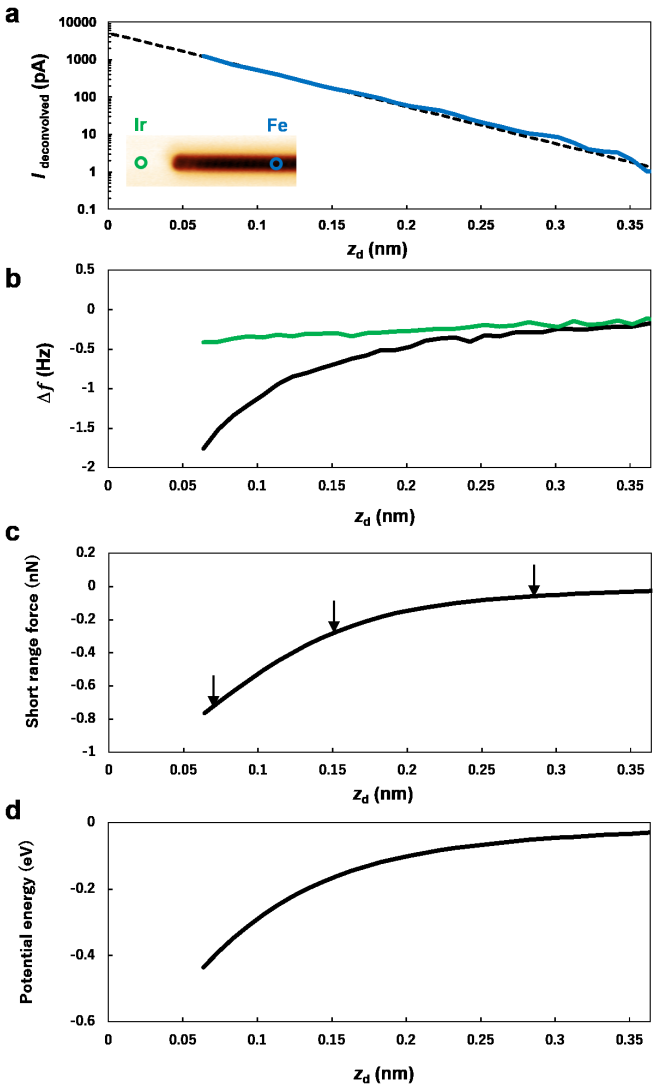

Fig. 3 (a) Tunneling current $I_{\mathrm{deconvolved}}$ (z_{d}) after deconvolution of the tip oscillation from $I(z_{\mathrm{d}})$. The black dotted line indicates exponential fitting. (b) $\Delta f_{\mathrm{Fe\,chain}}$ (z_{d}) simultaneously recorded with (a) (black solid curve). Δf_{Ir} (z_{d}) obtained on top of the Ir surface (green solid curve). Tip position is indicated by circles with green (Ir surface) and blue (Fe chain) in the inset image in (a). (a,b) are obtained by the Fe tip at $V = 65\,\mu\mathrm{V}$, $T = 4.5\,\mathrm{K}$ and $B = 3.0\,\mathrm{T}$. (c) Short-range force F_{SR} (z_{d}) obtained on top of the Fe chain. The arrows indicate the height where Fig. 4(b,c), Fig. 4(d,e), and Fig. 4(f,g) were obtained. (d) Potential energy U (z_{d}) obtained on top of the Fe chain.

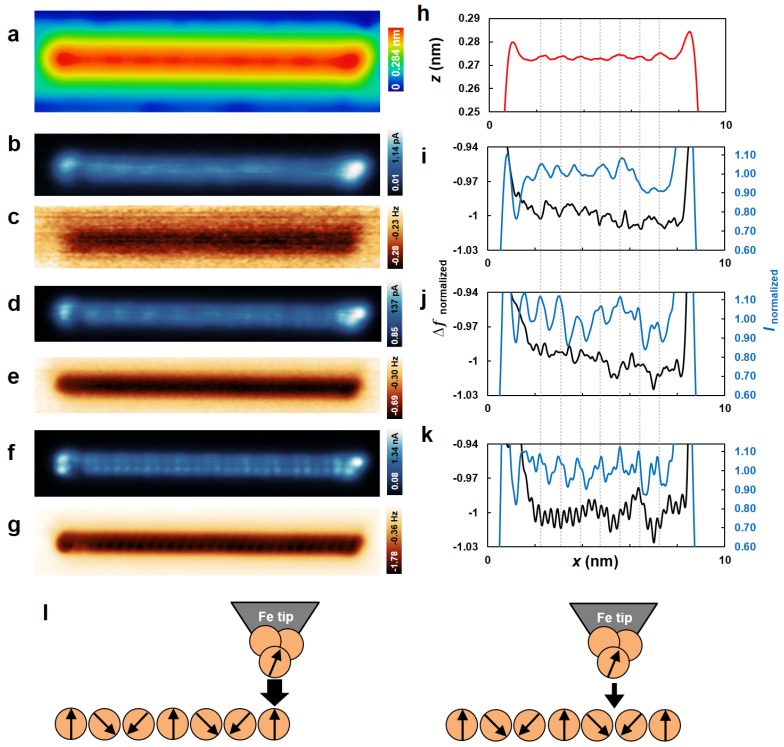

Fig. 4 (a) SP-STM topography image of Fe chain on Ir(001). Imaging condition: Constant-current mode. $V = 600\,\mathrm{mV}$, $I = 1.5\,\mathrm{nA}$, $T = 4.5\,\mathrm{K}$, $B = 3.0\,\mathrm{T}$. (b-g), Consecutive SP-STM (b, d, f) and MExFM images (c, e, g) of Fe chain on Ir(001). Imaging condition: Constant-height mode, $V = 65\,\mu\mathrm{V}$, $T = 4.5\,\mathrm{K}$ and $B = 3.0\,\mathrm{T}$, (b,c) $z_\mathrm{d} = 0.284\,\mathrm{nm}$; (d,e) $z_\mathrm{d} = 0.149\,\mathrm{nm}$; (f,g) $z_\mathrm{d} = 0.069\,\mathrm{nm}$. (h-k) Line profiles obtained along the chain axis shown in (a-g). The dashed lines across the line profiles are the guide for the lateral positions of the local maximum of the magnetic contrast in (h). (l) A schematic diagram that visually explains the interpretation. The left panel illustrates the case of strong ferromagnetic coupling, while the right panel shows the case of weak ferromagnetic coupling.

Notes and references

1 A. A. Khajetoorians, J. Wiebe, B. Chilian and R. Wiesendanger, *Science*, 2011, **332**, 1062–1064.

2 R. Elbertse, D. Coffey, J. Gobeil and A. Otte, *Communications Physics*, 2020, **3**, 94.

3 M. Menzel, Y. Mokrousov, R. Wieser, J. E. Bickel, E. Vedmedenko, S. Blügel, S. Heinze, K. von Bergmann, A. Kubetzka and R. Wiesendanger, *Physical review letters*, 2012, **108**, 197204.

4 S. Loth, S. Baumann, C. P. Lutz, D. Eigler and A. J. Heinrich, *Science*, 2012, **335**, 196–199.

5 R. Pawlak, M. Kisiel, J. Klinovaja, T. Meier, S. Kawai, T. Glatzel, D. Loss and E. Meyer, *npj Quantum Information*, 2016, **2**, 1–5.

6 H. Kim, A. Palacio-Morales, T. Posske, L. Rózsa, K. Palotás, L. Szunyogh, M. Thorwart and R. Wiesendanger, *Science Advances*, 2018, **4**, eaar5251.

7 A. Kamlapure, L. Cornils, J. Wiebe and R. Wiesendanger, *Nature communications*, 2018, **9**, 3253.

8 L. Schneider, S. Brinker, M. Steinbrecher, J. Hermenau, T. Posske, M. dos Santos Dias, S. Lounis, R. Wiesendanger and J. Wiebe, *Nature communications*, 2020, **11**, 4707.

9 E. Vedmedenko and D. Altwein, *Physical Review Letters*, 2014, **112**, 017206.

10 G. Yu, P. Upadhyaya, K. L. Wong, W. Jiang, J. G. Alzate, J. Tang, P. K. Amiri and K. L. Wang, *Physical Review B*, 2014, **89**, 104421.

11 M. Wu, T. Chen, T. Nomoto, Y. Tserkovnyak, H. Isshiki, Y. Nakatani, T. Higo, T. Tomita, K. Kondou, R. Arita *et al.*, *Nature Communications*, 2024, **15**, 4305.

12 Z. Luo, A. Hrabec, T. P. Dao, G. Sala, S. Finizio, J. Feng, S. Mayr, J. Raabe, P. Gambardella and L. J. Heyderman, *Nature*, 2020, **579**, 214–218.

13 R. Wiesendanger, *Reviews of Modern Physics*, 2009, **81**, 1495.

14 U. Kaiser, A. Schwarz and R. Wiesendanger, *Nature*, 2007, **446**, 522–525.

15 F. Pielmeier and F. J. Giessibl, *Physical review letters*, 2013, **110**, 266101.

16 R. Schmidt, C. Lazo, H. Holscher, U. Pi, V. Caciuc, A. Schwarz, R. Wiesendanger and S. Heinze, *Nano Letters*, 2009, **9**, 200–204.

17 R. Schmidt, C. Lazo, U. Kaiser, A. Schwarz, S. Heinze and R. Wiesendanger, *Phys. Rev. Lett.*, 2011, **106**, 257202.

18 C. Lazo, V. Caciuc, H. Hölscher and S. Heinze, *Phys. Rev. B*, 2008, **78**, 214416.

19 N. Hauptmann, J. W. Gerritsen, D. Wegner and A. A. Khajetoorians, *Nano letters*, 2017, **17**, 5660–5665.

20 J. Grenz, A. Köhler, A. Schwarz and R. Wiesendanger, *Phys. Rev. Lett.*, 2017, **119**, 047205.

21 N. Hauptmann, S. Haldar, T.-C. Hung, W. Jolie, M. Gutzeit, D. Wegner, S. Heinze and A. A. Khajetoorians, *Nature Communications*, 2020, **11**, year.

22 N. Hauptmann, M. Dupé, T.-C. Hung, A. K. Lemmens, D. Wegner, B. Dupé and A. A. Khajetoorians, *Physical Review B*, 2018, **97**, 100401.

23 I. M. Billas, A. Chatelain and W. A. de Heer, *Science*, 1994, **265**, 1682–1684.

24 H. J. Terunobu Miyazaki, *The Physics of Ferromagnetism*, Springer, 2012.

25 S. Blundell, *Magnetism in condensed matter*, OUP Oxford, 2001.

26 C.-W. Chen, *Magnetism and metallurgy of soft magnetic materials*, Courier Corporation, 2013.

27 J. C. Slater, *Physical review*, 1930, **36**, 57.

28 T. Moriya, *Progress of Theoretical Physics*, 1965, **33**, 157–183.

29 M. Menzel, A. Kubetzka, K. von Bergmann and R. Wiesendanger, *Physical Review Letters*, 2014, **112**, 047204.

30 R. Mazzarello and E. Tosatti, *Phys. Rev. B*, 2009, **79**, 134402.

31 M. Menzel, *PhD thesis*, University of Hamburg, 2011.

32 J. Yu, C. Urdaniz, Y. Namgoong and C. Wolf, *New Journal of Physics*, 2023, **25**, 113035.

33 L. Hammer, W. Meier, A. Schmidt and K. Heinz, *Phys. Rev. B*, 2003, **67**, 125422.

34 S. Yan, D.-J. Choi, J. A. Burgess, S. Rolf-Pissarczyk and S. Loth, *Nature nanotechnology*, 2015, **10**, 40–45.

35 Y. Sugimoto, K. Ueda, M. Abe and S. Morita, *Journal of Physics: Condensed Matter*, 2012, **24**, 084008.

36 J. E. Sader and Y. Sugimoto, *Applied Physics Letters*, 2010, **97**, year.

37 J. E. Sader and S. P. Jarvis, *Applied physics letters*, 2004, **84**, 1801–1803.

38 Y. Sugimoto, P. Pou, M. Abe, P. Jelinek, R. Pérez, S. Morita and O. Custance, *Nature*, 2007, **446**, 64–67.

39 M. Lantz, H.-J. Hug, R. Hoffmann, P. Van Schendel, P. Kappenberger, S. Martin, A. Baratoff and H.-J. Guntherodt, *Science*, 2001, **291**, 2580–2583.

40 M. Ternes, C. González, C. P. Lutz, P. Hapala, F. J. Giessibl, P. Jelínek and A. J. Heinrich, *Physical review letters*, 2011, **106**, 016802.

41 K. Tao, V. S. Stepanyuk, W. Hergert, I. Rungger, S. Sanvito and P. Bruno, *Phys. Rev. Lett.*, 2009, **103**, 057202.

42 C. Zener, *Physical Review*, 1951, **81**, 440.

43 C. Zener, *Physical Review*, 1951, **82**, 403.

The data supporting this article have been included as part of the Supplementary Information.